Research Article

Analysis of a Two-Regime Stochastic Car-Following Model: Explaining Capacity Drop and Oscillation Instabilities

Tu Xu[1] and Jorge A. Laval[1]

This paper presents analysis of a Newell-type stochastic car-following model based on stochastic desired acceleration processes. This formulation was shown to generalize previous efforts based on Brownian and geometric Brownian acceleration processes, each reproducing a different feature of the traffic instabilities. Here, we show that the unified model is able to capture virtually all types of traffic instabilities consistently with empirical data, including formation and propagation of oscillations, capacity drop in the absence of lane changes and the concave growth pattern of vehicle speeds along a platoon.

Stop-and-go traffic oscillations and capacity drop at bottlenecks have long been correlated with lane changing activity (*1–11*). However, it has been observed that these phenomena can occur in the absence of lane changing (*12–14*), and a convincing explanation for these phenomena is still lacking. It has been argued that a small driving instability may grow into mature traffic oscillations in the absence of lane changing (*15–19*) owing to the string instabilities in the mathematical models. On the other hand, Laval and Leclercq, and Chen et al. argue that heterogeneous driving behavior can cause the formation and propagation of traffic oscillations, but at the expense of several additional parameters (*20–22*).

A more parsimonious explanation for this phenomenon started with Laval et al., in which most traffic instabilities can be explained simply by the random nature of drivers' errors with the addition of a single variance parameter (*23*). Delpiano et al. proposed a social force car-following model implementation of this theory that includes finite decelerations (*24*). However, this parsimonious model was found to be unable to replicate the capacity drop in the absence of lane changes as observed empirically in Yuan et al. (*8*), and a reformulation of this model was proposed in their subsequent research (*14*). Recently, Xu and Laval noted that the model proposed in the research conducted by Yuan et al. loses the ability

to replicate the simulation formation and growth under some circumstances, and proposed a unified theory able to replicate both oscillation and capacity (*14, 25*). They also proposed a parameter estimation method that allows for performing statistical inference, but a comprehensive analysis of the properties of the model is missing.

The purpose of this paper is to undertake a detailed analysis of the unified model, and show that it is able to replicate many types of traffic instabilities consistently with empirical data, including oscillations, capacity drop and the concave growth pattern of vehicle speeds along a platoon, as recently reported by Jiang et al. (*26*). To this end, this paper is organized as follows. We first present the formulation and the estimated parameter values of the model. Then an analysis of the model properties including platoon oscillation growth, periodic oscillation at bottlenecks, capacity drop, and prediction of the vehicle speed in the middle of the platoon. Finally, a discussion is provided.

Background

The model to be analyzed in this paper was recently proposed by Xu and Laval(*25*) and generalizes previous research efforts as mentioned in the introduction (*14, 23, 24*). The model is a two-regime stochastic car-following model that can be thought of an extension of Newell's simplified car-following theory (*27*). It is expressed as the minimum of a free-flow term expressing the location (Y) that the vehicle can achieve when unobstructed by traffic, and a congestion term giving the most downstream location (Z) that the vehicle can safely achieve without colliding with its leader. It can be formulated as:

[1]Georgia Institute of Technology, Atlanta, GA

Corresponding Author:
Address correspondence to Jorge A. Laval: jorge.laval@ce.gatech.edu

Table 1. Parameter Value Estimation Results

Parameter	Estimated value	t-statistic
μ_τ	0.62	3.3
μ_δ	4.94	3.8
β	80	96.8
m	9.8	6.1
$\tilde{\sigma}$	0.020	5.8
σ_τ	0.24	0.6
σ_δ	2.27	1.0

$$x_j(t) = \min\{\underbrace{x_j(t - \tau) + \xi_j(\tau)}_{\text{free-flow}(Y)}, \; \underbrace{x_{j-1}(t - \tau) - \delta}_{\text{congestion}(Z)}\}, \quad (1)$$

in which $x_j(t)$ is the position of j-th vehicle at time t, τ is the wave trip time between two consecutive vehicle trajectories in congestion, δ is the jam spacing and $\xi_j(\tau)$ is a stochastic process describing the desired displacement of vehicle j during $t - \tau$ and t. It should be noted that τ is typically taken as the time step of the car-following model. The congestion term Z is approximately normally distributed after assuming: (i) a approximately constant leader speed during a time step, and (ii) that parameters τ and δ follow the bivariate normal (BVN) distribution with correlation $\rho = 0$, as demonstrated empirically by Ahn et al. (28), that is:

$$(\tau, \delta) \sim BVN(\mu_\tau, \mu_\delta, \sigma_\tau, \sigma_\delta, \rho)$$

in which μ and σ are the mean and standard deviation of the variable in subscript.

The free-flow term Y is also normally distributed because $\xi_j(\tau)$ is a stochastic process describing the desired displacement of vehicle j during $t - \tau$ and t, and which corresponds to the integral of the speed. This free-flow acceleration process can be formulated as:

$$\begin{cases} d\xi(t) = v(t)dt, \quad \xi(0) = 0, & (2a) \\ dv(t) = (v_c - v(t))\beta dt + (mv_c - v(t))\sigma dW(t), \; v(0) = v_0, & (2b) \end{cases}$$

in which $v(t)$ is the current vehicle speed, v_c is the desired speed, β is the inverse relaxation time, m is a dimensionless parameter and mv_c represents the speed at which the standard deviation of the driver acceleration is zero, $W(t)$ is a standard Brownian motion and σ is its diffusion coefficient. One can solve the equation analytically and show that $\xi_j(\tau)$ follows approximately a normal distribution. The parameter m provides a scale from the geometric Brownian motion (g-BM) model reported by Yuan et al. ($m = 1$) to the original Brownian motion (BM) model reported by Laval et al. ($m \gg 1$) (14, 23). A dimensionless formulation of (2) reveals that the only two non-observable parameters that drive this model are m and $\tilde{\sigma}^2 = \sigma^2/\beta$.

Finally, as random processes Y and Z are normally distributed: $Y \sim N(\mu_Y, \sigma_Y)$, $Z \sim N(\mu_Z, \sigma_Z)$, one can show that the probability density function of $x_j(t), f(x; \Theta)$, given the data up to time t and the set of model parameters $\Theta = (u, \mu_\tau, \mu_\delta, \beta, m, \tilde{\sigma}, \rho, \sigma_\tau, \sigma_\delta)$ is given by

$$f(x; \Theta) =$$

$$\frac{1}{2\sqrt{2\pi}} \left(\frac{1}{\sigma_Z} e^{-\frac{(\mu_Z - x)^2}{2\sigma_Z^2}} \text{erfc}\left(\frac{x - \mu_Y}{\sqrt{2}\sigma_Y}\right) + \frac{1}{\sigma_Y} e^{-\frac{(\mu_Y - x)^2}{2\sigma_Y^2}} \text{erfc}\left(\frac{x - \mu_Z}{\sqrt{2}\sigma_Z}\right) \right)$$

$$(3)$$

in which erfc $(x) = \frac{2}{\sqrt{\pi}} \int_x^\infty e^{-t^2} dt$ is the complementary error function. The mean and standard deviations of the free-flow and congestion terms are given by:

$$\begin{cases} \mu_Y = x_j(t_i - \tau') + \text{E}[\xi(\tau')], & (4a) \\ \sigma_Y = \text{SD}[\xi(\tau')], & (4b) \\ \mu_Z = x_{j-1}(t_i - \mu_\tau) - \mu_\delta, & (4c) \\ \sigma_Z = \sqrt{v_{j-1}^2(t_i)\sigma_\tau^2 + \sigma_\delta^2 + 2\rho v_{j-1}^2(t_i)\sigma_\tau^2\sigma_\delta^2}. & (4d) \end{cases}$$

which is all we need to evaluate (3) and use maximum likelihood estimation (MLE) to estimate the parameters.

Data Set

In this paper, we used the data from the previous paper published by Jiang et al., who conducted a car-following experiment with 25 passenger cars with homogeneous vehicle lengths that are all equipped with data collection devices (26). In this experiment, the vehicle platoon traveled northbound and southbound repeatedly, on a two-way 3.5 km suburban road segment in Hefei, China. The grade data is also contained in the dataset. In the experiments, the lead vehicle was required to maintain a given constant speed and the other vehicles were expected to follow the leader naturally. There was no interference from traffic signals or other vehicles in the experiments.

Instead of using the parameter values obtained from the research conducted by Ahn et al., we estimate the parameter values (28). The parameter estimation methodology was introduced in a previous publication by Xu and Laval (25). Unless otherwise indicated, most of the experiments presented here use the parameters estimated from this dataset, which are summarized in Table 1.

Model Properties

In this section, we undertake a detailed analysis of the unified model and show that it is able to replicate virtually all types of traffic instabilities consistently with empirical data, including oscillations, capacity drop, hysteresis, and the concave growth pattern of vehicle speeds along a platoon, as recently reported (26).
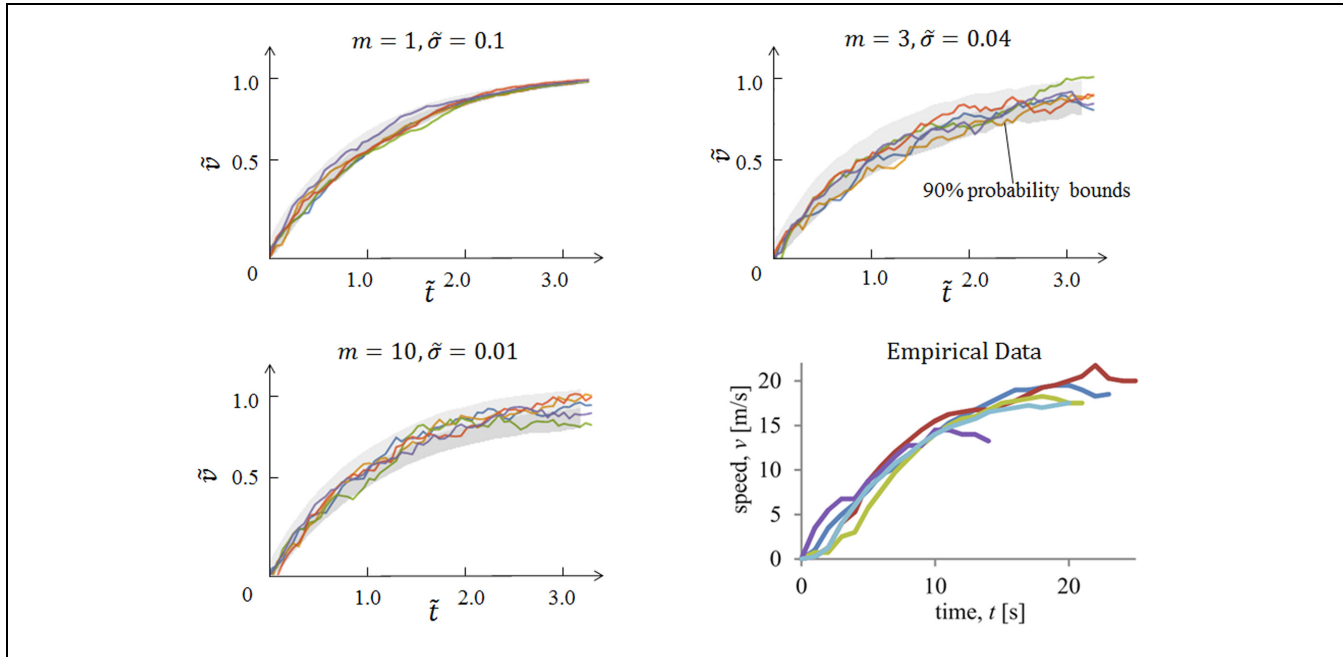
Figure 1. Five realizations along with the 90% probability bounds for the acceleration process starting from $\tilde{v}_0 = 0$ along with empirical vehicle acceleration data from Laval et al. (23). In the figures, each line represents each acceleration process and the gray area represents the 90% probability bounds.

Physical Bounds on the Parameters $m, \tilde{\sigma}$

As with any normally distributed random variable there is always a probability that it will be negative. Following on from the previous research, for the worst case scenario $v(0) = 0$, we need $P\{v(\beta\tau) \leqslant 0\} \leqslant \alpha$, for a small prescribed α (23). For typical values of $\beta \approx 0.07$ s^{-1} and $\tau \approx 1.2$ s and $\alpha = 0.1$, one has:

$$m\tilde{\sigma} \leqslant 0.23$$

Which is a secure range of parameter values for the acceleration process starting from a complete stop. If a negative speed is realized in the simulation, it should be set to 0.

Free-Flow Acceleration Process

In this section we analyze the variability of the free-flow acceleration process (2). To eliminate irrelevant parameters from this analysis, we can formulate the key variables of this model in the dimensionless form. One possibility is the following transformations:

$$\tilde{t} = \beta t, \quad \tilde{v}(\tilde{t}) = v(\tilde{t})/v_c, . \quad \tilde{\sigma}^2 = \sigma^2/\beta. \qquad (5)$$

in which dimensionless variables are indicated with a tilde.

Figure 1 shows five realizations of the free-flow acceleration process (2) along with the 90% probability bounds, for different values of the model parameters. All three combinations of the parameter values capture the exponential growth of the vehicle speed during the acceleration process, but they all exhibit different variabilities. As a reference, the figure also includes the empirical data from Laval et al. (23).

The speed variability can be measured by the coefficient of variation of the dimensionless speed: $C[\tilde{v}(\tilde{t})] = V[\tilde{v}(\tilde{t})]^{1/2}/E[\tilde{v}(\tilde{t})]$. we present $C[\tilde{v}(\tilde{t})]/(m\tilde{\sigma})$ in Figure 2, which shows that most of the speed variability occurs at the beginning of an acceleration process, that is, for $\tilde{v}_0 < 0.5$ but converges for all values of $\tilde{v}_0$. It can be shown that this value is almost independent of $\tilde{\sigma}$ and also independent of m for large m s. One can then find that $C[\tilde{v}(\tilde{t})]$ converges to $\frac{(m-1)\tilde{\sigma}}{\sqrt{2-\sigma^2}}$. For a g-BM model, that is, $m = 1$, the variability of speed converges to 0. For a BM model, that is, $m \gg 1, \tilde{\sigma} \leqslant \frac{0.23}{m} \approx 0$, the value $C[\tilde{v}(\tilde{t})]/(m\tilde{\sigma})$ converges to $\frac{(m-1)\tilde{\sigma}}{m\tilde{\sigma}\sqrt{2-\sigma^2}} \approx \sqrt{0.5}$, which corresponds well with the results reported by Laval et al. (23). A similar analysis shows that the position variability converges to 0 regardless of the initial speed.

These results indicate that regardless of the parameter values, the speed variability is maximal at the beginning of the acceleration process and that it slowly converges to a value between 0 and $\sqrt{1/2}$ as time passes.
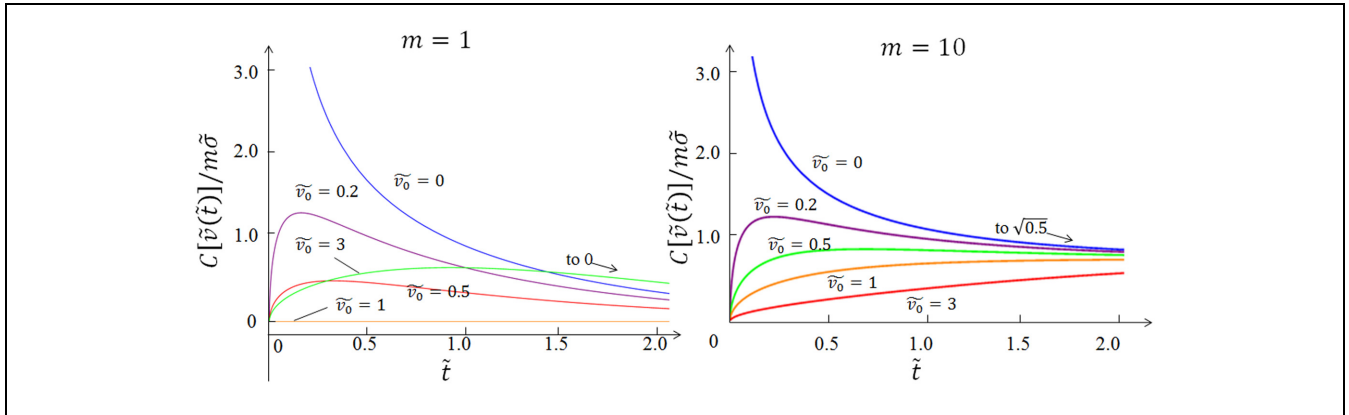
Figure 2. Rescaled coefficient of variation for the dimensionless speed $\tilde{v}(\tilde{t})$ for several values of the initial speed $\tilde{v}_0$.

Concave Growth of Platoon Oscillation

The concave growth of the vehicle platoon oscillation was first observed by Jiang et al. (26). Tian et al. found that the growth pattern in different oscillations collapses into a single concave curve, which indicates the law of the oscillation growth is universal (29). Treiber and Kesting showed that the Brownian motion model in Laval et al., and the intelligent driver model (IDM) model with noise and indifference regions are all able to reproduce the concave growth pattern, strongly indicating that a stochastic component is vital for replicating this important phenomena (19, 23).

Here, we show that the model analyzed in this paper is also able to reproduce the concave growth of the platoon oscillation, as seen in Figure 3. The left column in the figure corresponds to the model results with parameters from Table 1, in which it can be seen that the fit deteriorates for low lead vehicle speeds. The right column in the figure correspond to the same parameter values except for m and $\tilde{\sigma}$ which were chosen to optimize the fit with the data. This shows that the proposed model reproduces the concave growth of platoon oscillation, and that the parameters m and $\tilde{\sigma}$ dictate the shape of the growth.

We also conducted a 300-vehicle car-following simulation experiment that shows that the speed standard deviation first increases with the vehicle index in a concave way and then stabilizes; as seen in Figure 4. This result is consistent with previous research (14, 30).

It is interesting to investigate the maximum oscillation amplitude and also the number of vehicles (stable vehicle index) taken to stop the oscillation growth; see Figure 4. We conducted simulations with different lead vehicle speeds and model parameters. It is shown that the maximum oscillation amplitude is an increasing function of the lead vehicle speed, almost independent of the model parameters. In the meantime, the stable vehicle index

increases with v_{lead} and decreases with the production of $m\tilde{\sigma}$. This relationship is visualized in Figure 5.

Periodic Oscillation at Uphill Bottlenecks

In this section, we study the effects of the parameters m and $\tilde{\sigma}$ on the period and amplitude of the oscillations produced by the model, and compare them with empirical data. We conducted simulations on a 600 m one-lane flat road, except for a 100 m uphill segment starting at location $x = 400$ m. To take the roadway grade into account, one can express the desired speed as $v_c = u - gG/\beta$, in which $g = 9.81$ m/s^2 is the acceleration of gravity and G is the grade expressed as a decimal. A free-flow speed of $u = 120$ km/h was used for the simulations and for varying the parameters β, G, m and $\tilde{\sigma}$ within their typical ranges. Then we used Fourier spectrum analysis to estimate the period and amplitude of the speed series oscillations 100 m upstream of the bottom of the upgrade, as suggested in the previous research (23, 31).

Figure 6 shows the distribution of dimensionless periods (period times β) and dimensionless amplitudes (amplitude divided by v_c) as a function of $m\tilde{\sigma}$ and the average speed at the start of the uphill segment, V_{avg}. It can be seen that: (i) the dimensionless period is a decreasing function of $m\tilde{\sigma}$ and the dimensionless amplitude is an increasing function of $m\tilde{\sigma}$; (ii) the distribution of the dimensionless period and the dimensionless amplitude as a function of V_{avg} agrees well with the empirical data reported previously (18, 32); and (iii) all distributions exhibit a large variance. These results are similar to those reported previously, except that the relationship between the dimensionless period and amplitude are correlated with $m\tilde{\sigma}$ and not simply $\tilde{\sigma}$ (23).

The relationship between V_{avg} and $m\tilde{\sigma}$ is presented in Figure 7. V_{avg} decreases with $m\tilde{\sigma}$. Again, this result is similar to that reported in previous research, except that V_{avg}
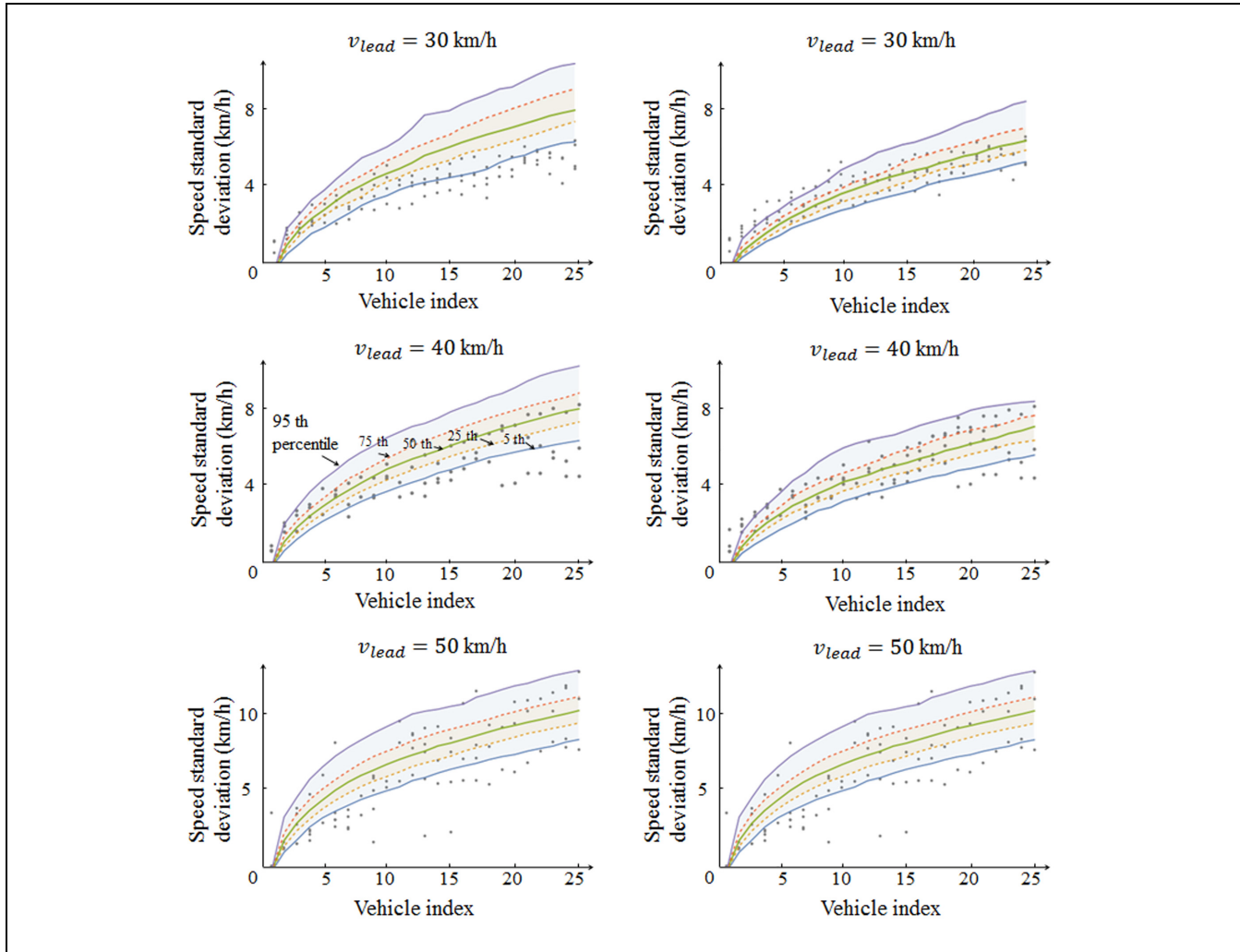
Figure 3. Simulated speed standard deviations for 25 vehicles in a vehicle platoon. The leading vehicle drives at $v_{lead} = 30$ km/h, $v_{lead} = 40$ km/h, and $v_{lead} = 50$ km/h. The gray dots are obtained from Jiang's car-following experiments (*26*). The probability bounds in the left column are generated from the estimated parameter values in Table 1 and those in the right column are generated using the selected parameter values. The selected values are $m = 1.25$, $\tilde{\sigma} = 0.165$ for $v_{lead} = 30$ km/h and $v_{lead} = 40$ km/h, and the selected values are the same as the estimated values for $v_{lead} = 50$ km/h.
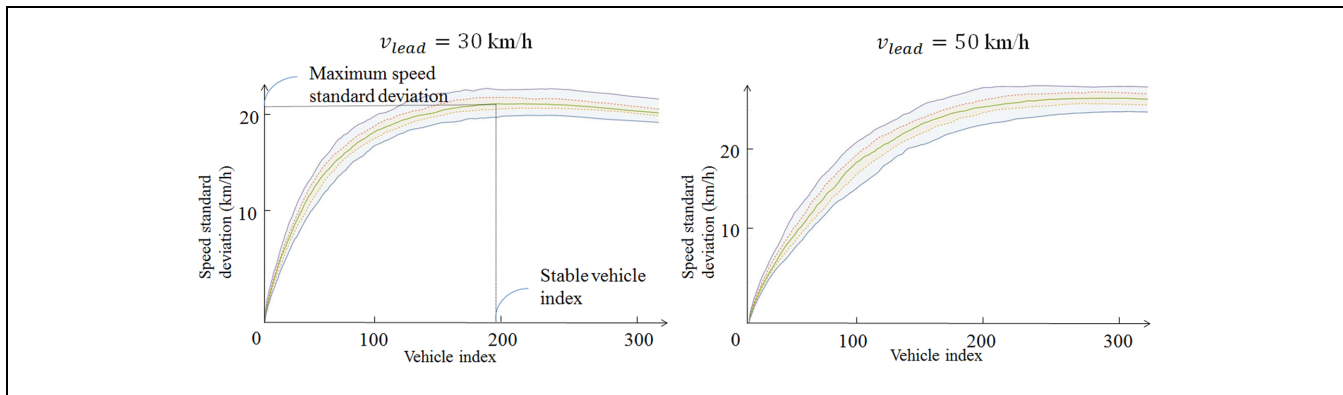

Figure 4. Simulated speed standard deviations for 25 vehicles in a vehicle platoon. The leading vehicle drives at $v_{lead} = 30$ km/h (*left column*) and $v_{lead} = 50$ km/h (*right column*). Parameter values are $m = 1.25$, $\tilde{\sigma} = 0.176$. The lines in the figures represents the 5th, 25th, 50th, 75th and 95th percentile of the realizations.
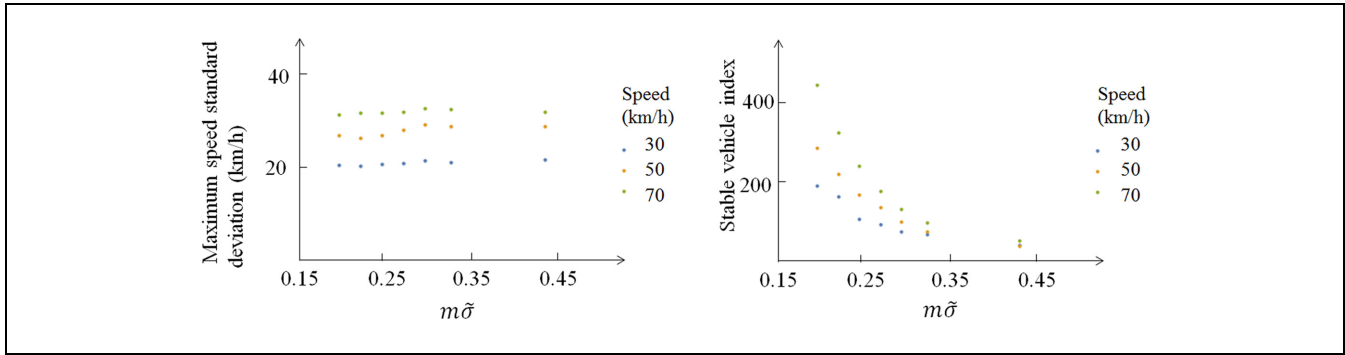
Figure 5. Relationship between the maximum speed variation (*left column*), the stable vehicle index (*right column*) and the v_{lead}, $m\tilde{\sigma}$. Here the speed process does not start with $\tilde{v}(0) = 0$ therefore we can accept a larger range of $m\tilde{\sigma}$ than mentioned in the previous section.
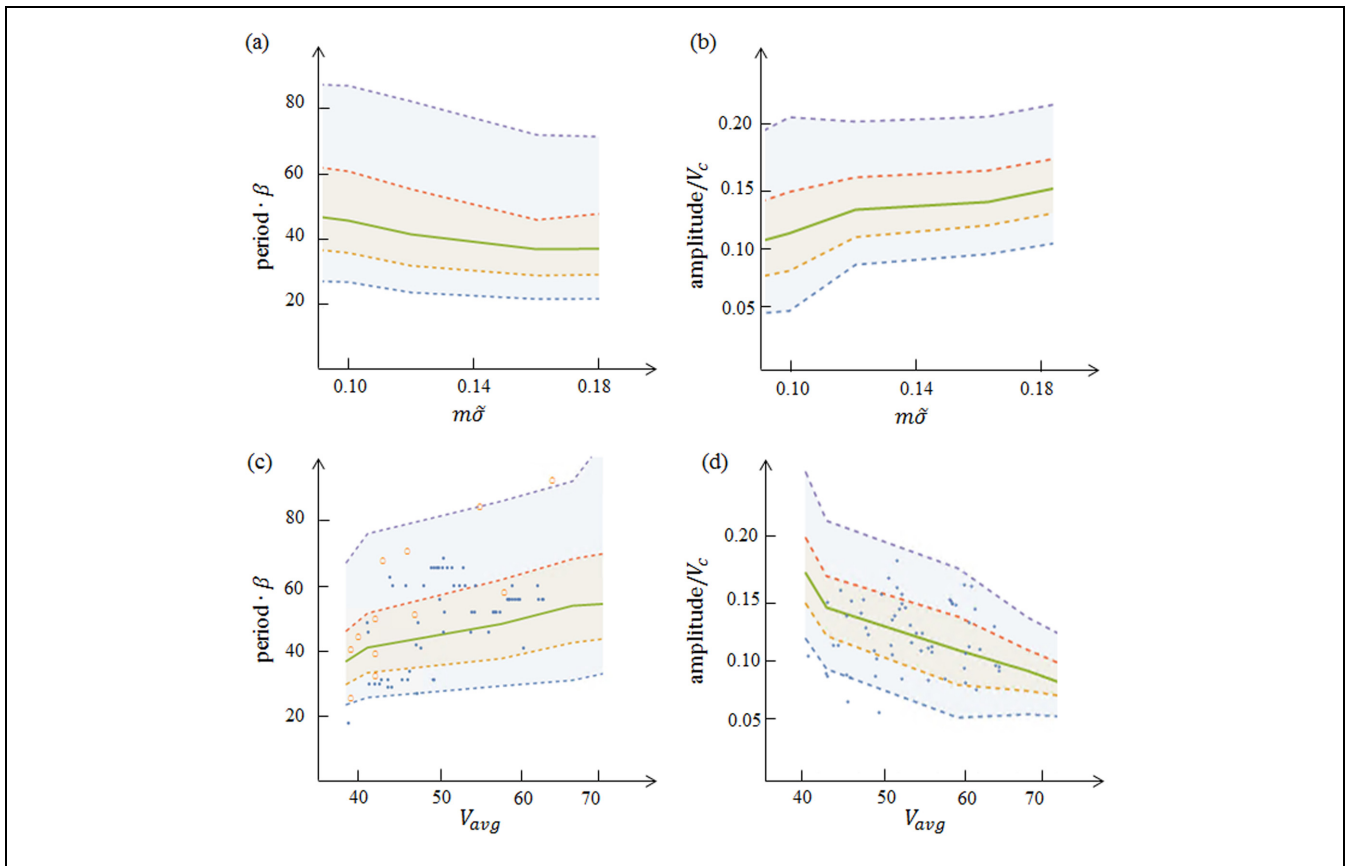

Figure 6. (a)(b) The dimensionless period and the dimensionless amplitude as a function of the model parameter $m\tilde{\sigma}$. (c)(d) The dimensionless period and the dimensionless amplitude as a function of V_{avg}. The lines represent the 5th, 25th, 50th, 75th and 95th percentile of the simulation results. The orange circles in part (c) are empirical data originally taken from (*18*) and the blue dots in part (c) and (d) are taken from previous research (*32*). To convert the empirical data into the dimensionless form we used $w = 18$ km/h, $\beta = 0.07$ s^{-1} and the following linear regression on the simulated data: $v_c = 3.6V_{avg} - 71.4$.

is correlated with $m\tilde{\sigma}$ but not only $\tilde{\sigma}$ (*23*). This indicates that the average speed at the bottleneck decreases with the randomness of driver accelerations.

Speed-Capacity Relationship in Congestion

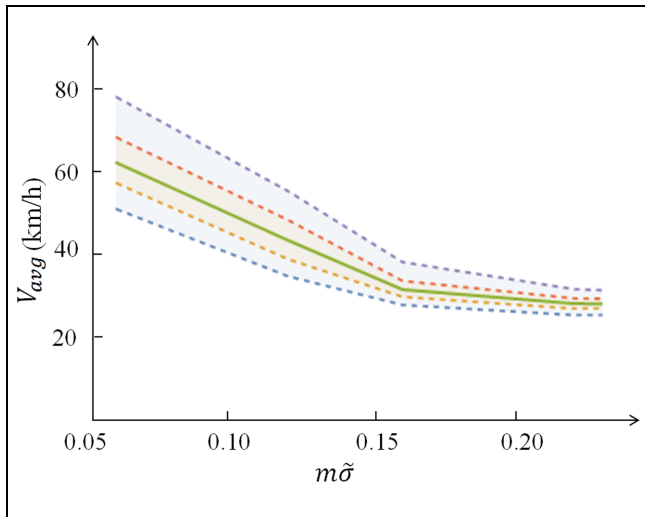Recent empirical findings reported by Yuan et al. show that the queue discharge rate out of a moving jam

Figure 7. Average speed at the bottom of the uphill segment as a function of $m\tilde{\sigma}$. The lines represent the 5th, 25th, 50th, 75th and 95th percentile of the simulation results.
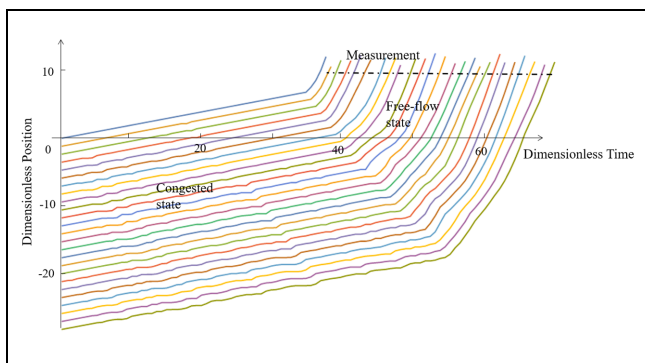

Figure 8. A sample trajectory of the queue discharge experiment with $\tilde{v}_0 = 0.1$, $m = 1.25$, and $\tilde{\sigma} = 0.35$. The initial spacing of the vehicles is calculated based on the triangular fundamental diagram $\rho = \delta + \tilde{v}_0\tau$. The discharge rate is measured at the black dash line at which the vehicle speeds reach free flow speed.

increases with the speed in the queue (8). On average, they observed that the capacity drop magnitude is around 26% if the vehicular speed in congestion is 0 km/h and decreases as the vehicular speed increases. The mechanisms behind this "speed-capacity" relationship were recently unveiled by Yuan et al. (14): the key ingredients are bounded vehicle acceleration and an error term that decreases with the speed. As noted earlier, the geometric Brownian motion model reported previously reproduces this phenomenon for the first time, but loses the ability to generate realistic traffic oscillations (14). The model analyzed in this paper does not have this drawback, as shown below.

We performed a simulation of a 25-vehicle car-following experiment on a one-lane road with no

passing, in which the lead vehicle drives initially at a constant low speed, then accelerates to free-flow speed, the resulting discharge rate was measured at that location, as seen in Figure 8.

Figure 9 plots the results, in which it can be seen that the model is able to successfully reproduce the increasing speed-capacity relationship and that the slope of this increasing relationship is inversely proportional to m. This is as expected as small values of m mean that the model is closer to the geometric Brownian motion model.

The important point here, is that a value of $m \approx 1.2$ is able to replicate both the speed-capacity relationship and realistic traffic oscillations. To observe this, the speed-capacity relationship is shown in Figures 9 and 10, and an example of the realization of traffic oscillations is provided in Figure 11.

We also found that the queue discharge rate decreases with $\tilde{\sigma}$ for the same values of m and $\tilde{v}$, two examples are provided in Figure 10. As we can see, for $m = 1.25$ and $\tilde{v} = 0.6$, the corresponding dimensionless queue discharge rates are approximately 0.95, 0.91 and 0.87 for $\tilde{\sigma} = 0.15$, 0.25, and 0.35.

Vehicle Speed Distributions

Here we use repeated simulations of the same scenario to approximate the speed distribution of each vehicle $n = 1, 2, \ldots$ in a platoon, in which the trajectory of the leader $n = 1$ is taken from empirical data. We use two datasets: (i) from Jiang et al. as mentioned above, and (ii) from Laval et al. who performed a similar car-following experiment on a two-lane road close to Georgia Tech with six vehicles (23, 26). The grade data was also provided. For both of the datasets, the realizations of the follower speeds (15th vehicle for dataset 1, and 6th vehicle for dataset 2) fall into the probability bands and the width of the probability band is a function of $m\tilde{\sigma}$. Examples are provided in Figure 12. In the predictions, the trajectories of the platoon leader and the initial conditions of all followers were provided. Then, we ran simulations repeatedly to obtain distributions of the predicted vehicle speed.

Discussion

This paper analyzes the properties of the model proposed by Xu and Laval, which is an extension to previously conductedworks (14, 23, 25). The extension is achieved by adding a dimensionless parameter m which regulates the type of driver error on a scale from Brownian to geometric Brownian acceleration processes. A suitable value of m, that is, $m \approx 1.2$, can allow the model to reproduce the best features of the BM and g-BM models, namely realistic traffic oscillations and the speed-capacity relationship. Furthermore, this model also captures the
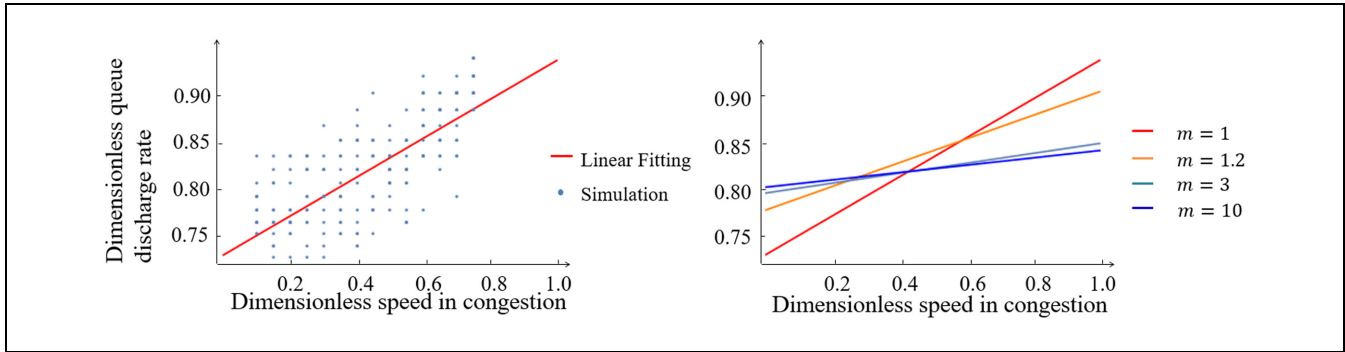
Figure 9. (*a*) Simulation results and a linear fitting of the desired model with the parameter $m = 1$, which shows a positive relationship between the queue discharge rate and speed in congestion, and (*b*) dimensionless queue discharge rate as a function of the dimensionless speed in congestion for $m \in \{1, 1.2, 3, 10\}$. The model gradually loses its ability to reflect the positive relationship between the speed and queue discharge rate with the increase of the value of m. The dimensionless queue discharge rate is the ratio of the queue discharge rate to the roadway capacity.
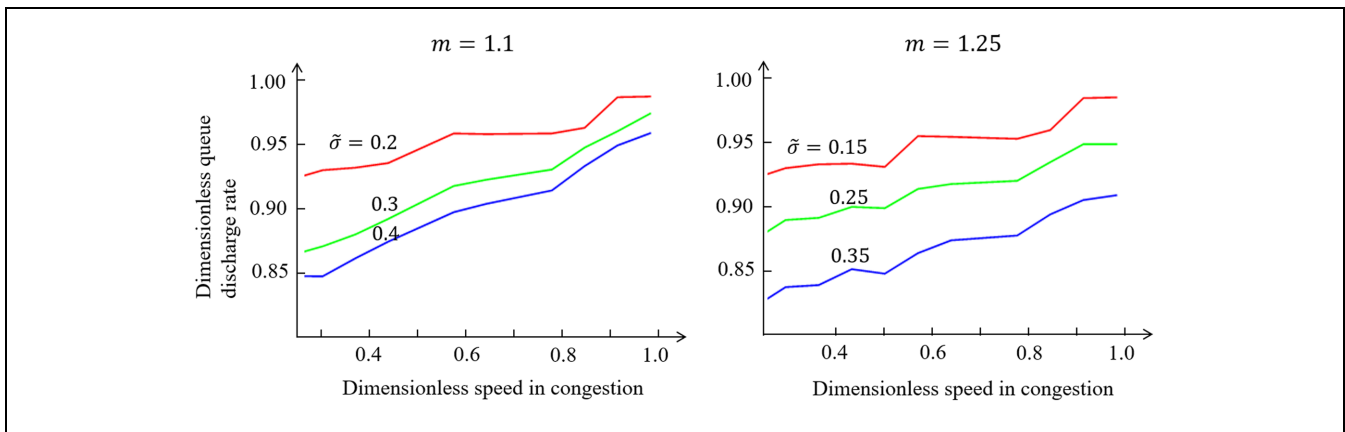

Figure 10. Dimensionless queue discharge rate as a function of speed for different values of $\tilde{\sigma}$. In the figures, we can observe that for the same speed, the queue discharge rate decreases with $\tilde{\sigma}$.
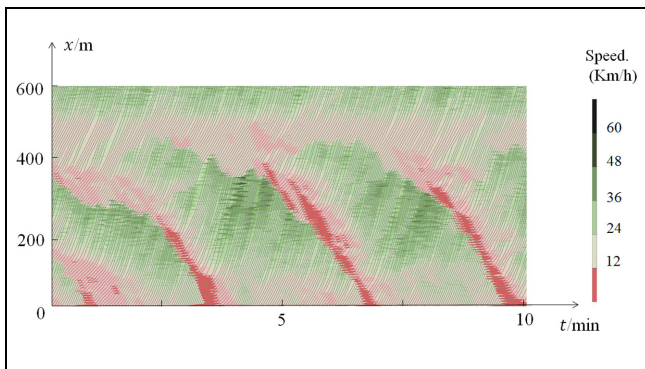

Figure 11. An example of the realistic traffic oscillations generated using the proposed model. The model parameters are $m = 1.2$ and $\tilde{\sigma} = 0.16$.

concave growth of the platoon oscillation and predicts the distributions of the vehicle speeds well. For the concave growth pattern of the vehicle platoon, we find that the growth pattern is influenced by the lead vehicle speed and the model parameter $m\tilde{\sigma}$.

Parameters m and $\tilde{\sigma}$ are the two parameters that control the model performance according to the dimensionless formulation of the model. However, the parameter values of m and $\tilde{\sigma}$ are not universal and need to be calibrated in different regions. To do this, we can first try to use MLE to estimate the model parameter values if the vehicle platoon data is available. If we only have the loop detector data, we can calculate the period and amplitude of the traffic oscillation from the speed series and then refer to Figure 6 to solve the local value of $m\tilde{\sigma}$.

The product of m and $\tilde{\sigma}$ has a big impact on the model. It determines: (i) the oscillation period and amplitude; (ii) the average speed at the bottleneck; (iii) the discharge rate at the bottleneck; (iv) the stable vehicle index of the concave growth of the platoon oscillation; and (v) the width of the probability band of the predicted vehicle speed.
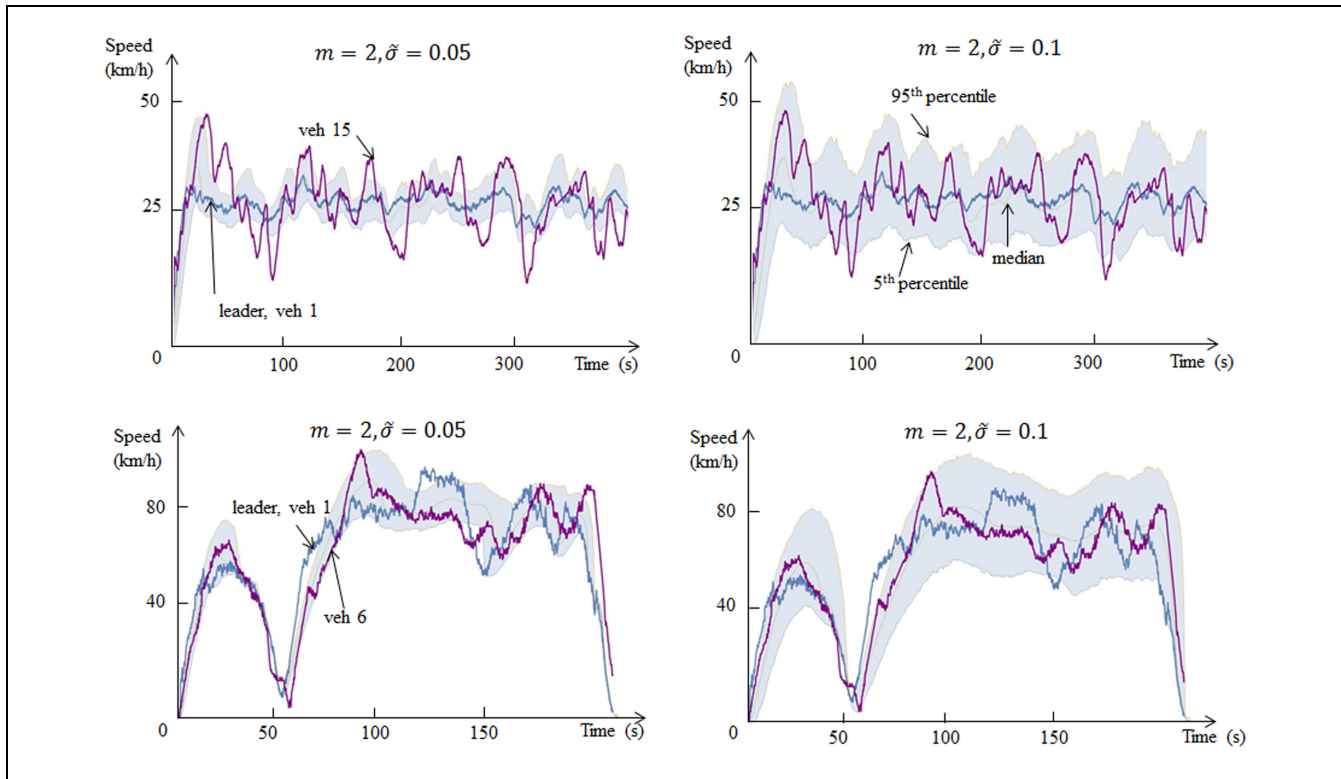
Figure 12. Results of car-following experiments using initial data from Jiang et al. (*top row*) and Laval et al. (*bottom row*) (*23, 26*). The observed speeds for the leader and the vehicles are shown in solid lines. The shaded area represents the 90%-probability band of the predicted vehicle speed. The vehicle speed curve has been shifted to the left by the wave trip time between the two vehicles.

If we are trying to replicate the concave oscillation growth and predict the vehicle speed distributions with the estimated parameter values found in Table 1, we find some deviation from empirical data and this deviation depends on the platoon lead vehicle speed. This means the methodology for the parameter estimation reported in Xu and Laval could be improved to incorporate these other types of performance measures (*25*). Alternatively, instead of estimating the parameters with vehicle pairs (1st, 2nd), (2nd, 3rd)...(*i* th, *i* + 1 th)..., we can instead use a constant leader, that is, (1st, 2nd), (1st, 3rd)...(1st, *i* th)...This method may give us better results while predicting the vehicle speed distributions with the estimated parameter values.

The current work is limited to homogeneous vehicle lengths, as Coifman indicates that the vehicle length has an impact on the parameters τ and δ, and traffic waves travel at different speed across vehicles of different lengths (*33*). In the future, we plan to accommodate our model to fit a situation in which vehicle lengths are heterogeneous.

Author Contributions

The authors confirm contribution to the paper as follows: study conception and design: JAL, TX; data analysis: TX; interpretation of results: TX, JAL; draft manuscript preparation: TX,

JAL. Both authors reviewed the results and approved the final version of the manuscript.

References

1. Mauch, M., and M. J. Cassidy. Freeway Traffic Oscillations: Observations and Predictions. In *Proc., 15th International Symposium on Transportation and Traffic Theory in the 21st Century* (M. Taylor ed.), Pergamon-Elsevier, Oxford, 2002, pp. 653–673.
2. Laval, J. A. Linking Synchronized Flow and Kinematic Wave Theory. In *Traffic and Granular Flow '05* (T. Schadschneider, A. Poschel, R. Kuhne, M. Schreckenberg, and D. Wolf, eds.), Springer, Berlin, Heidelberg, 2005, pp. 521–526.
3. Laval, J. A., and C. F. Daganzo. Lane-Changing in Traffic Streams. *Transportation Research Part B: Methodological*, Vol. 40, No. 3, 2006, pp. 251–264.
4. Ahn, S., and M. Cassidy. Freeway Traffic Oscillations and Vehicle Lane-Change Manoeuvres. In *17th International Symposium on Transportation and Traffic Theory* (B. Heydecker, M. Bell, and R. Allsop eds.), Elsevier, New York, 2007, pp. 691–710.
5. Zheng, Z., S. Ahn, D. Chen, and J. Laval. Applications of Wavelet Transform for Analysis of Freeway Traffic: Bottlenecks, Transient Traffic, and Traffic Oscillations. *Transportation Research Part B: Methodological*, Vol. 45, No. 2, 2011, pp. 372–384.

6. Coifman, B., and S. Kim. Extended Bottlenecks, the Fundamental Relationship, and Capacity Drop on Freeways. *Transportation Research Part A: Policy and Practice*, Vol. 45, No. 9, 2011, pp. 980–991.

7. Leclercq, L., J. A. Laval, and N. Chiabaut. Capacity Drops at Merges: An Endogenous Model. *Procedia -Social and Behavioral Sciences*, Vol. 17, 2011, pp. 12–26.

8. Yuan, K., V. L. Knoop, and S. P. Hoogendoorn. Capacity Drop: Relationship between Speed in Congestion and the Queue Discharge Rate. *Transportation Research Record: Journal of the Transportation Research Board*, 2015. 2491: 72–80.

9. Chen, D., and S. Ahn. Capacity-Drop at Extended Bottlenecks: Merge, Diverge, and Weave. *Transportation Research Part B: Methodological*, Vol. 108, 2018, pp. 1–20.

10. Jin, W. L. A first-Order Behavioral Model of Capacity Drop. *Transportation Research Part B: Methodological*, Vol. 105, 2017, pp. 438–457.

11. Kontorinaki, M., A. Spiliopoulou, C. Roncoli, and M. Papageorgiou. First-Order Traffic Flow Models Incorporating Capacity Drop: Overview and Real-Data Validation. *Transportation Research Part B: Methodological*, Vol. 106, 2017, pp. 52–75.

12. Sugiyama, Y., M. Fukui, M. Kikuchi, K. Hasebe, A. Nakayama, K. Nishinari, S.-I. Tadaki, and S. Yukawa. Traffic Jams without Bottlenecks-Experimental Evidence for the Physical Mechanism of the Formation of a Jam. *New Journal of Physics*, Vol. 10, 2008, p. 033001.

13. Oh, S., and H. Yeo. Impact of Stop-and-Go Waves and Lane Changes on Discharge Rate in Recovery Flow. *Transportation Research Part B: Methodological*, Vol. 77, 2015, pp. 88–102.

14. Yuan, K., J. Laval, V. L. Knoop, R. Jiang, and S. Hoogendoorn. A Geometric Brownian Motion Car-Following Model: Towards a Better Understanding of Capacity Drop. *Transportmetrica B*, 2018, forthcoming.

15. Treiber, M., A. Hennecke, and D. Helbing. Derivation, Properties, and Simulation of a GasKinetic-Based, Non-Local Traffic Model. *Physical Review E*, Vol. 59, 1999, pp. 239–253.

16. Wilson, R. E. Mechanisms for Spatio-Temporal Pattern Formation in Highway Traffic Models. *Philosophical Transactions of the Royal Society A: Mathematical, Physical and Engineering Sciences*, Vol. 1872, 2008, pp. 2017–2032.

17. Wilson, R., and J. Ward. Car-Following Models: Fifty Years of Linear Stability Analysis -A Mathematical Perspective. *Transportation Planning and Technology*, Vol. 34, No. 1, 2011, pp. 3–18.

18. Treiber, M., and A. Kesting. Validation of Traffic Flow Models with Respect to the Spatiotemporal Evolution of Congested Traffic Patterns. *Transportation Research Part C: Emerging Technologies*, Vol. 21, No. 1, 2012, pp. 31–41.

19. Treiber, M., and A. Kesting. The Intelligent Driver Model with Stochasticity -New Insights into Traffic Flow Oscillations. *Transportation Research Procedia*, Vol. 23, 2017, pp. 174–187.

20. Laval, J. A., and L. Leclercq. A Mechanism to Describe the Formation and Propagation of Stop-and-Go Waves in Congested Freeway Traffic. *Philosophical Transactions of the Royal Society A*, Vol. 368, No. 1928, 2010, pp. 4519–4541.

21. Chen, D., J. Laval, Z. Zheng, and S. Ahn. A Behavioral Car-Following Model that Captures Traffic Oscillations. *Transportation Research Part B: Methodological*, Vol. 46, No. 6, 2012, pp. 744–761.

22. Chen, D., J. A. Laval, S. Ahn, and Z. Zheng. Microscopic Traffic Hysteresis in Traffic Oscillations: A Behavioral Perspective. *Transportation Research Part B: Methodological*, Vol. 46, No. 10, 2012, pp. 1440–1453.

23. Laval, J. A., C. S. Toth, and Y. Zhou. A Parsimonious Model for the Formation of Oscillations in Car-Following Models. *Transportation Research Part B: Methodological*, Vol. 70, 2014, pp. 228–238.

24. Delpiano, R., J. Laval, J. E. Coeymans, and J. C. Herrera. The Kinematic Wave Model with finite Decelerations: A Social Force Car-Following Model Approximation. *Transportation Research Part B: Methodological*, Vol. 71, 2015, pp. 182–193.

25. Xu, T., and J. A. Laval. Parameter Estimation of a Stochastic Microscopic Car-Following Model. Presented at 97th Annual Meeting of the Transportation Research Board, Washington, D.C., 2018.

26. Jiang, R., M. B. Hu, H. M. Zhang, Z. Y. Gao, B. Jia, Q. S. Wu, B. Wang, and M. Yang. Traffic Experiment Reveals the Nature of Car-Following. *PLoS One*, Vol. 9, No. 4, 2014, pp. 1–9.

27. Newell, G. F. A Simplified Car-Following Theory: A Lower Order Model. *Transportation Research Part B: Methodological*, Vol. 36, No. 3, 2002, pp. 195–205.

28. Ahn, S., M. Cassidy, and J. A. Laval. Verification of a Simplified Car-Following Theory. *Transportation Research Part B: Methodological*, Vol. 38, No. 5, 2003, pp. 431–440.

29. Tian, J., R. Jiang, B. Jia, Z. Gao, and S. Ma. Empirical Analysis and Simulation of the Concave Growth Pattern of Traffic Oscillations. *Transportation Research Part B: Methodological*, Vol. 93, 2016, pp. 338–354.

30. Li, X., and Y. Ouyang. Characterization of Traffic Oscillation Propagation under Nonlinear Car-Following Laws. *Procedia -Social and Behavioral Sciences*, Vol. 17, 2011, pp. 663–682.

31. Li, X., F. Peng, and Y. Ouyang. Measurement and Estimation of Traffic Oscillation Properties. *Transportation Research Part B: Methodological*, Vol. 44, No. 1, 2010, pp. 1–14.

32. Knoop, V., C. Buisson, E. Wilson, and B. Van Arem. Number of Lane Changes Determined by Splashover Effects in Loop Detector Counts. *Transactions on Intelligent Transportation Systems*, Vol. 13, No. 4, 2012, pp. 1525–1534.

33. Coifman, B. Empirical Flow-Density and Speed-Spacing Relationships: Evidence of Vehicle Length Dependency. *Transportation Research Part B: Methodological*, Vol. 78, 2015, pp. 54–65.